

A sound-sensitive neuron incorporating a memristive-ion channel

Xin-Lin Song(宋欣林), Ge Zhang(张鬲), and Fei-Fei Yang(杨飞飞)
Citation: Chin. Phys. B, 2025, 34 (**12**): 120502. DOI: 10.1088/1674-1056/ae0563
http://cpb.iphy.ac.cn; http://iopscience.iop.org/cpb

What follows is a list of articles you may be interested in

Synchronous dynamics of robotic arms driven by Chua circuits

Guoping Sun(孙国平), Mingxin Xu(许明鑫), Guoqiang Jin(金国强), and Xufeng Wang(王旭峰)
Chin. Phys. B, 2025, 34 (**6**): 060501. DOI: 10.1088/1674-1056/adc2e1

Memristors-coupled neuron models with multiple firing patterns and homogeneous and heterogeneous multistability

Xuan Wang(王暄), Santo Banerjee, Yinghong Cao(曹颖鸿), and Jun Mou(牟俊)
Chin. Phys. B, 2024, 33 (**10**): 100501. DOI: 10.1088/1674-1056/ad6256

Dynamics and synchronization of neural models with memristive membranes under energy coupling

Jingyue Wan(万婧玥), Fuqiang Wu(吴富强), Jun Ma(马军), and Wenshuai Wang(汪文帅)
Chin. Phys. B, 2024, 33 (**5**): 050504. DOI: 10.1088/1674-1056/ad1dcc

Characteristic analysis of 5D symmetric Hamiltonian conservative hyperchaotic system with hidden multiple stability

Li-Lian Huang(黄丽莲), Yan-Hao Ma(马衍昊), and Chuang Li(李创)
Chin. Phys. B, 2024, 33 (**1**): 010503. DOI: 10.1088/1674-1056/acf9e7

Dynamical analysis, geometric control and digital hardware implementation of a complex-valued laser system with a locally active memristor

Yi-Qun Li(李逸群), Jian Liu(刘坚), Chun-Biao Li(李春彪), Zhi-Feng Hao(郝志峰), and Xiao-Tong Zhang(张晓彤)
Chin. Phys. B, 2023, 32 (**8**): 080503. DOI: 10.1088/1674-1056/acd68b

---

SPECIAL TOPIC — Biophysical circuits: Modeling & applications in neuroscience

A sound-sensitive neuron incorporating a memristive-ion channel

Xin-Lin Song(宋欣林)[1], Ge Zhang(张鬲)[1], and Fei-Fei Yang(杨飞飞)[2,†]

[1] *College of Science, Xi'an University of Science and Technology, Xi'an* 710054, *China*

[2] *College of Artificial Intelligence and Computer Science, Xi'an University of Science and Technology, Xi'an* 710054, *China*

(Received 5 August 2025; revised manuscript received 8 September 2025; accepted manuscript online 10 September 2025)

The nonlinear memory characteristics of memristors resemble those of biological synapses and ion channels. Therefore, memristors serve as ideal components for constructing artificial neurons. This paper presents a sound-sensitive neuron circuit featuring a memristor-based hybrid ion channel, designed to simulate the dynamic response mechanisms of biological auditory neurons to acoustic signals. In this neural circuit, a piezoelectric ceramic element captures external sound signals, while the hybrid ion channel is formed by connecting a charge-controlled memristor in series with an inductor. The circuit realizes selective encoding of sound frequency and amplitude and investigates the influence of external electric fields on neuronal ion-channel dynamics. In the dynamic analysis, bifurcation diagrams and Lyapunov exponents are employed to reveal the rich nonlinear behaviors, such as chaotic oscillations and periodic oscillations, exhibited by the circuit during the acoustic–electric conversion process, and the validity of the circuit model is experimentally verified. Simulation results show that by adjusting the threshold of the ratio between electric-field energy and magnetic-field energy, the firing modes and parameters of neurons can be adaptively regulated. Moreover, the model exhibits stochastic resonance in noisy environments. This research provides a theoretical foundation for the development of new bionic auditory sensing hardware and opens a new path for the bio-inspired design of memristor–ion-channel hybrid systems.

Keywords: sound-sensitive neuron, hybrid memristor ion channel, Hamilton energy

PACS: 05.45.–a, 84.30.–r

DOI: 10.1088/1674-1056/ae0563 **CSTR:** 32038.14.CPB.ae0563

1. Introduction

With the rapid development of neuromorphic computing and bionic electronics, the modeling and design of functional neural circuits have received extensive attention. The biological nervous system possesses efficient, parallel, and low-power information processing capabilities. However, traditional computing systems based on the von Neumann architecture encounter bottlenecks in terms of energy efficiency and real-time performance when handling complex perception tasks (such as sound recognition and visual processing). Therefore, constructing electronic circuits that can simulate the dynamic behaviors of biological neurons has become one of the key research directions for achieving next-generation brain-like intelligent hardware.

From a physical perspective, the basic components of simple neural circuits mainly include capacitors, inductors, resistors, and nonlinear resistors. The incorporation of functional electronic elements into simple neuronal circuits enables the implementation of dedicated neural processing functions. For example, adding a phototube into a simple neural circuit results in a light-sensitive neuron[1] capable of capturing external light signals. A thermistor can be connected to a simple neural circuit to construct a temperature-sensitive neuron[2] for sensing external temperature. A piezoelectric ceramic element can be introduced into a simple neural circuit to design a speech neuron[3] for encoding external sound signals. Additionally, the simultaneous integration of a phototube and a thermistor into a simple neural circuit yields a functional neural model that can sense both external temperature and light.[4,5]

The nonlinear memory characteristics of memristors[6–9] resemble those of biological synapses and ion channels.[10] Therefore, memristors serve as ideal components for constructing neurons.[11–13] For instance, magnetic-field-sensitive neurons,[14–16] electric-field-sensitive neurons,[17] electromagnetic-field-sensitive neurons,[18,19] memristive membrane neurons,[20–22] memristive ion-channel neurons,[23–25] and memristor neuron maps[26–28] have all been implemented based on memristor circuits. In addition, many memristor-based neurons have been constructed by introducing memristors into neuron models governed by differential equations, such as memristive FitzHugh–Nagumo (FHN) neurons[29–31] and memristive map neurons.[32–34] A comprehensive survey of memristor-based neuronal modeling can be found in the review.[35] Furthermore, numerous functional neurons have been coupled to investigate synchronization characteristics,[36–38] energy balance,[39,40] heterogeneity,[41] defects,[42] and pattern formation.[43–45]

[†]Corresponding author. E-mail: yangfeifei@xust.edu.cn

© 2025 Chinese Physical Society and IOP Publishing Ltd. All rights, including for text and data mining, AI training, and similar technologies, are reserved.

Auditory neurons possess characteristics such as frequency selectivity and adaptive gain control. Achieving these functions at the circuit level remains an open challenge. Moreover, existing studies have rarely explored the impact of synergistic interactions between memristors and ion channels on the dynamic behavior of neurons, which is crucial for constructing functional neuronal circuits with greater biological fidelity. This paper presents a functional neuronal circuit model based on memristor hybrid ion channels, focusing on its dynamic characteristics in sound-signal perception and encoding. This circuit can simulate the frequency selectivity, adaptive firing behavior, and noise robustness observed in biological auditory neurons. We employ nonlinear dynamic analysis methods to investigate its working mechanisms. This research not only provides new hardware design strategies for neuromorphic computing but also offers theoretical insights into the perception–computation integration mechanisms of biological neurons. The main contributions of this study are summarized as follows.

(i) A sound-sensitive neuron circuit incorporating a memristive-ion channel is presented based on a memristive nonlinear circuit.

(ii) The encoding of sound frequency and amplitude, as well as the effects of external electric fields on neuronal ion channels, is investigated using the proposed sound-sensitive neuron circuit.

(iii) An adaptive growth method for a key parameter based on the energy ratio is proposed.

In this paper, the model of the sound-sensitive neuron is described in Section 2. In Section 3, the dynamic behavior of the sound-sensitive neuron is analyzed. The conclusions and perspectives are presented in Section 4.

2. Model of a sound-sensitive neuron

A functional neural circuit can be built by connecting a functional electronic component to a typical neuron circuit. An external sound signal can be converted into an electrical signal through a piezoelectric ceramic element. Therefore, this paper proposes a sound-sensitive neural circuit by applying a piezoelectric ceramic element, a nonlinear resistor, a capacitor, an inductor, a charge-controlled memristor, and a linear resistor. Figure 1 shows the schematic diagram of the proposed sound-sensitive neural circuit.

A hybrid memristor-based ion channel is implemented by connecting a charge-controlled memristor in series with an inductor. The charge-controlled memristor is selected as follows:[13]

$$\begin{cases} V_{\mathrm{M}} = M(q) I_{\mathrm{M}} = k_{\mathrm{M}} \left(\alpha + 3\beta q^2\right) I_{\mathrm{M}}, \\ \dfrac{\mathrm{d}q}{\mathrm{d}t} = aq + bI_{\mathrm{M}}, \end{cases} \tag{1}$$

where (k_{M}, a, b, α, β) denote the parameters related to the memristor material, and (V_{M}, I_{M}, q) represent the voltage, current, and charge in the memristor. The fourth branch circuit in Fig. 1 is described by

$$I_{\mathrm{N}} = -\frac{1}{\rho}\left(V - \frac{V^3}{3V_0^2}\right), \tag{2}$$

where ρ denotes resistance, V_0 is the reverse cut-off voltage, and (I_{N}, V) represent the current and voltage in the nonlinear resistor. For the piezoelectric ceramic, the deformation effect caused by the external mechanical pressure F can be expressed through the output voltage at both ends of the piezoelectric ceramic. They are described as follows:

$$\begin{cases} V_{\mathrm{PC}} = V_{\mathrm{PC}}(F, \mu) = \dfrac{F}{S}\dfrac{d_0}{\varepsilon} h = P\sigma h, \\ \sigma = \dfrac{d_0}{\varepsilon}, \ \ d_0 = \dfrac{Q}{F}, \end{cases} \tag{3}$$

where (Q, S, h, ε) denote the charge released by the piezoelectric ceramic, its cross-sectional area, its thickness, and the dielectric constant of the medium, respectively. By applying Kirchhoff's laws, the circuit equations in Fig. 1 can be expressed as

$$\begin{cases} C\dfrac{\mathrm{d}V}{\mathrm{d}t} = \dfrac{V_{\mathrm{PC}} - V}{R_{\mathrm{S}}} - I_{\mathrm{N}} - I_{\mathrm{L}}, \\ L\dfrac{\mathrm{d}I_{\mathrm{L}}}{\mathrm{d}t} = V - k_{\mathrm{M}}\left(\alpha + 3\beta q^2\right) I_{\mathrm{L}}, \\ \dfrac{\mathrm{d}q}{\mathrm{d}t} = aq + bI_{\mathrm{L}}. \end{cases} \tag{4}$$

Equation (4) represents a dimensional model of the dynamics. For a more detailed analysis, the variables in Eq. (4) are transformed into dimensionless form as follows:

$$x = \frac{V}{V_0}, \ \ y = \frac{\rho I_{\mathrm{L}}}{V_0}, \ \ z = \frac{q}{CV_0}, \ \ \tau = \frac{t}{\rho C}. \tag{5}$$

In addition, the parameters in Eq. (4) are defined by

$$\begin{aligned} &a' = a\rho C, \ \ c = \frac{\rho^2 C}{L}, \ \ d = \frac{\rho}{R_{\mathrm{S}}}, \\ &u_{\mathrm{PC}} = \frac{\rho V_{\mathrm{PC}}}{V_0 R_{\mathrm{S}}}, \ \ \alpha' = \frac{\alpha}{\rho}, \ \ \beta' = \frac{C^2 V_0^2}{\rho}\beta. \end{aligned} \tag{6}$$

Therefore, Eq. (4) can be rewritten in dimensionless form as

$$\begin{cases} \dfrac{\mathrm{d}x}{\mathrm{d}\tau} = u_{\mathrm{PC}} + (1-d)x - \dfrac{1}{3}x^3 - y, \\ \dfrac{\mathrm{d}y}{\mathrm{d}\tau} = c\left[x - k_{\mathrm{M}}\left(\alpha' + 3\beta' z^2\right) y\right], \\ \dfrac{\mathrm{d}z}{\mathrm{d}\tau} = a'z + by. \end{cases} \tag{7}$$

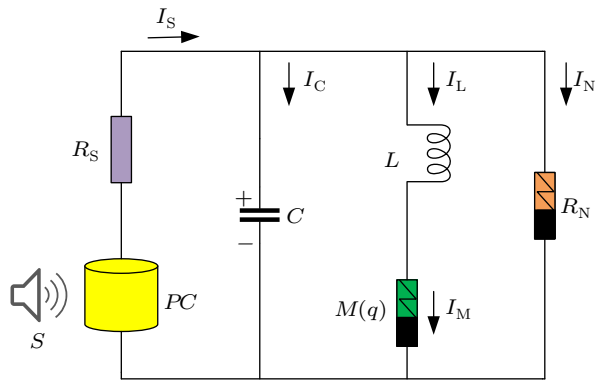


Fig. 1. A sound-sensitive neural circuit with a hybrid memristor–ion channel. S, R_N, L, R_s, PC, and C denote the sound signal source, the nonlinear resistor, inductor, linear resistor, piezoelectric ceramic, and capacitor element, respectively. $M(q)$ is a charge-controlled memristor.

The field energy and the dimensionless Hamilton energy displayed in Fig. 1 are determined through the following calculations:

$$\begin{cases} W = W_C + W_L + W_M = \dfrac{1}{2}CV^2 + \dfrac{1}{2}LI_L^2 + \dfrac{1}{2}qV_M, \\ H = \dfrac{W}{CV_0^2} = H_C + H_L + H_M \\ \quad = \dfrac{1}{2}x^2 + \dfrac{1}{2c}y^2 + \dfrac{1}{2}k_M zy\left(\alpha' + 3\beta' z^2\right). \end{cases} \tag{8}$$

Equation (8) indicates that the energy of the neural circuit depends on the circuit parameters and its output variables. Furthermore, Helmholtz's theorem is employed to validate the energy function of the neural circuit, and the verification process is described as follows:

$$\begin{aligned} \begin{pmatrix} \dot{x} \\ \dot{y} \\ \dot{z} \end{pmatrix} &= \begin{pmatrix} u_{PC} + (1-d)x - (1/3)x^3 - y \\ c\left[x - k_M\left(\alpha' + 3\beta' z^2\right)y\right] \\ a'z + by \end{pmatrix} = F_c + F_d \\ &= \begin{pmatrix} -y - 0.5ck_M\left(\alpha' z + 3\beta' z^3\right) \\ cx - 0.5cbyk_M\left(\alpha' + 9\beta' z^2\right) \\ by + 0.5cbk_M\left(\alpha' z + 3\beta' z^3\right) \end{pmatrix} \\ &\quad + \begin{pmatrix} u_{PC} + (1-d)x - (1/3)x^3 + 0.5ck_M\left(\alpha' z + 3\beta' z^3\right) \\ cyk_M\left[\alpha'(0.5b-1) + 3\beta' z^2(1.5b-1)\right] \\ a'z - 0.5cbk_M\left(\alpha' z + 3\beta' z^3\right) \end{pmatrix} \\ &= \begin{pmatrix} 0 & -c & 0 \\ c & 0 & -cb \\ 0 & cb & 0 \end{pmatrix} \begin{pmatrix} x \\ (1/c)y + 0.5k_M\left(\alpha' z + 3\beta' z^3\right) \\ 0.5yk_M\left(\alpha' + 9\beta' z^2\right) \end{pmatrix} \\ &\quad + \begin{pmatrix} n_{11} & 0 & 0 \\ 0 & n_{22} & 0 \\ 0 & 0 & n_{33} \end{pmatrix} \begin{pmatrix} x \\ (1/c)y + 0.5k_M\left(\alpha' z + 3\beta' z^3\right) \\ 0.5yk_M\left(\alpha' + 9\beta' z^2\right) \end{pmatrix}, \end{aligned}$$

$$n_{11} = \frac{u_{PC} + (1-d)x - (1/3)x^3 + 0.5ck_M\left(\alpha' z + 3\beta' z^3\right)}{x},$$

$$n_{22} = \frac{cyk_M\left[\alpha'(0.5b-1) + 3\beta' z^2(1.5b-1)\right]}{(1/c)y + 0.5k_M\left(\alpha' z + 3\beta' z^3\right)},$$

$$n_{33} = \frac{a'z - 0.5cbk_M\left(\alpha' z + 3\beta' z^3\right)}{0.5yk_M\left(\alpha' + 9\beta' z^2\right)}. \tag{9}$$

In fact, the energy expressions presented in Eq. (8) satisfy

$$\nabla H^{\mathrm{T}} F_c(x,y,z) = 0, \quad \nabla H^{\mathrm{T}} F_d(x,y,z) = \frac{\mathrm{d}H}{\mathrm{d}\tau}, \tag{10}$$

$$\begin{aligned} &\left[-y - 0.5ck_M\left(\alpha' z + 3\beta' z^3\right)\right]\frac{\partial H}{\partial x} \\ &+ \left[cx - 0.5cbyk_M\left(\alpha' + 9\beta' z^2\right)\right]\frac{\partial H}{\partial y} \\ &+ \left[by + 0.5cbk_M\left(\alpha' z + 3\beta' z^3\right)\right]\frac{\partial H}{\partial z} = 0. \end{aligned} \tag{11}$$

3. Results of numerical simulation

The nonlinear dynamical behaviors of the neuron model described by Eq. (7) are investigated through numerical simulations using MATLAB software. At first, the parameters are set as $a' = -0.1$, $b = 0.2$, $c = k_M = \alpha' = 0.1$, $d = 0.25$, and $\beta' = 0.01$, and the initial value is chosen as (0.0, 0.0, 0.1). The case of periodic external sound signals is examined, where u_{PC} is defined as $A\cos(f\tau)$. Figure 2 presents the bifurcation diagram of variable x and the largest Lyapunov exponent (LLE) under different amplitudes (A) and angular frequencies (f).

Figure 2 demonstrates that varying the external sound signal induces distinct dynamical characteristics (periodic and chaotic states) in the sound-sensitive neuron with hybrid memristor–ion channels. Additionally, Fig. 3 shows the corresponding firing patterns and energy evolution across different angular frequencies.

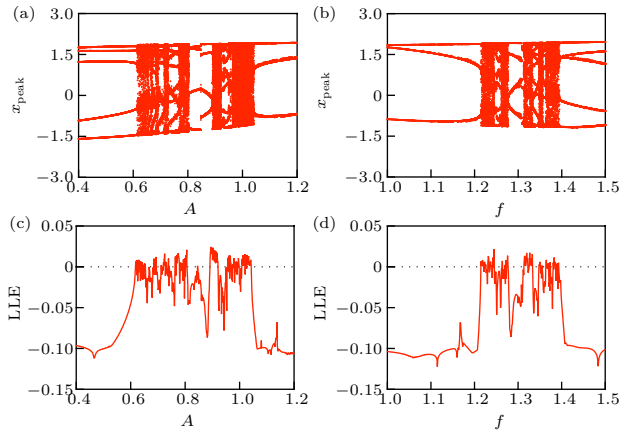


Fig. 2. Bifurcation diagram of the variable x (x_{peak}) and the LLE by adjusting the external sound signal. (a) and (c) $f = 1.23$; (b) and (d) $A = 1.0$.

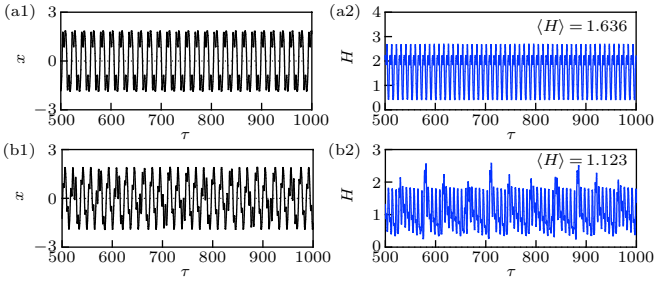


Fig. 3. The membrane potential (x) and the Hamilton energy (H) by adjusting f. (a1) and (a2) $A = 1.0$, $f = 1.0$; (b1) and (b2) $A = 1.0$, $f = 1.23$.

From Fig. 3, different firing patterns correspond to distinct energy time series and exhibit different energy distributions. For example, a chaotic pattern is associated with a lower average energy, whereas a periodic state maintains a higher mean energy. Therefore, the energy proportions corresponding to different firing modes obtained by adjusting f are illustrated in Fig. 4.

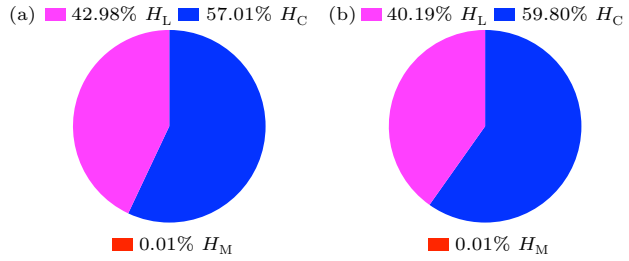


Fig. 4. The energy proportion under different f. (a) $A = 1.0$, $f = 1.0$; (b) $A = 1.0$, $f = 1.23$.

Figure 4 shows the relationship between the electric field energy and the magnetic field energy corresponding to different firing modes. It can be seen that the magnetic field energy proportion for periodic patterns is higher than that for the chaotic mode, whereas the electric field energy proportion for periodic patterns is lower than that for the chaotic mode. Meanwhile, the case of the external noise sound signal is plotted in Fig. 5.

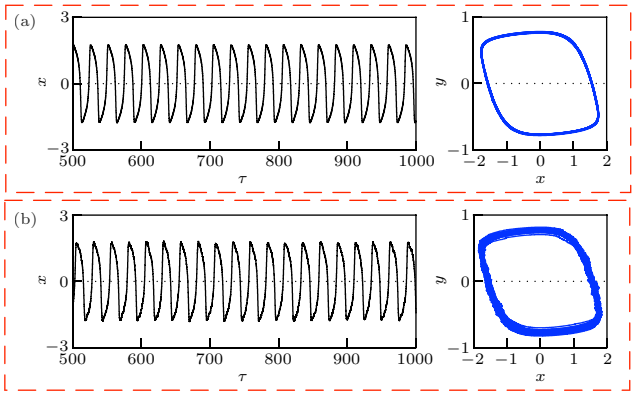


Fig. 5. The membrane potential (x) and the phase plane (x–y) under different external noise sound signal strengths D_0. (a) $D_0 = 0.02$; (b) $D_0 = 0.5$. D_0 represents the Gaussian white noise external sound signal strength.

Figure 5 shows the firing modes under different external noise sound signal strengths. The firing pattern for a weak external noise sound signal strength ($D_0 = 0.02$) is periodic, and with increasing D_0, it becomes quasi-periodic. In fact, a charge-controlled memristor can capture an external electric field in the nonlinear circuit. Thus, the sound-sensitive neuron incorporating a hybrid memristor–ion channel can be mathematically represented as follows:

$$\begin{cases} \dfrac{\mathrm{d}x}{\mathrm{d}\tau} = u_{\mathrm{PC}} + (1-d)x - \dfrac{1}{3}x^3 - y, \\ \dfrac{\mathrm{d}y}{\mathrm{d}\tau} = c\left[x - k_{\mathrm{M}}\left(\alpha' + 3\beta' z^2\right)y\right], \\ \dfrac{\mathrm{d}z}{\mathrm{d}\tau} = a'z + by + E_{\mathrm{ext}}, \end{cases} \tag{12}$$

where E_{ext} is an external electric field signal. The influence of constant external electric field signals on the dynamical behavior of the neuron is investigated. The same parameter set and initial conditions are preserved as in the preceding analysis. Figure 6 presents the bifurcation diagram of variable x for different sound signals under different intensities of constant external electric field signals.

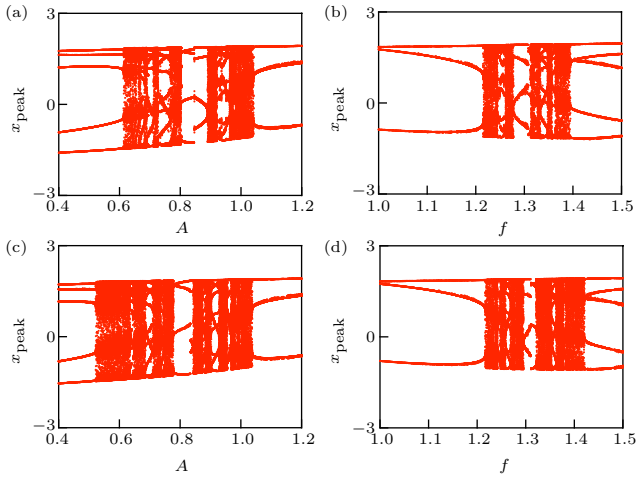


Fig. 6. Bifurcation diagram of the variable x for different constant external electric fields. (a) $E_{\mathrm{ext}} = 0.127$, $f = 1.23$; (b) $E_{\mathrm{ext}} = 0.127$, $A = 1.0$; (c) $E_{\mathrm{ext}} = 1.0$, $f = 1.23$; (d) $E_{\mathrm{ext}} = 1.0$, $A = 1.0$.

From the comparison of Figs. 2 and 6, it can be seen that a larger amplitude or frequency of the external sound signal triggers the chaotic mode of neurons. In addition, under a stronger external electric field interference, the amplitude and frequency ranges of the chaotic mode of neurons become larger. Similarly, the different firing patterns and energy evolution for different external electric fields and sound signals are shown in Fig. 7.

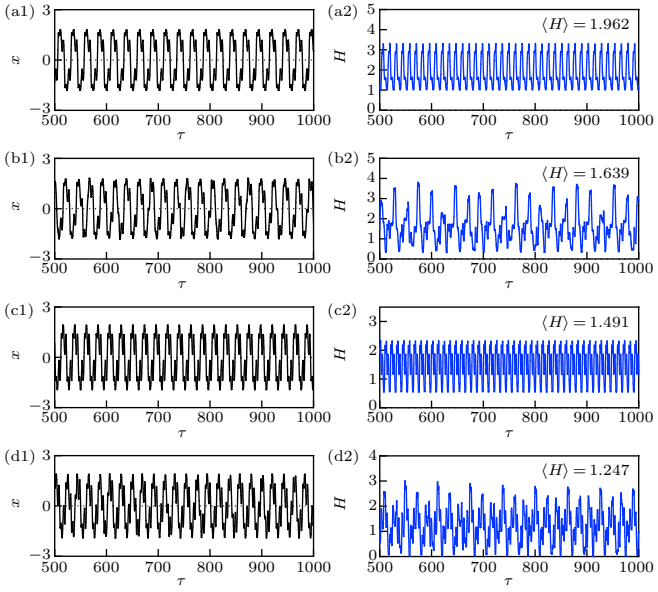


Fig. 7. The membrane potential (x) and the Hamilton energy (H) under different external electric fields and sound signals. (a1) and (a2) $E_{\mathrm{ext}} = 0.127$, $A = 0.6$, $f = 1.23$; (b1) and (b2) $E_{\mathrm{ext}} = 1.0$, $A = 0.6$, $f = 1.23$; (c1) and (c2) $E_{\mathrm{ext}} = 0.127$, $A = 1.0$, $f = 1.4$; (d1) and (d2) $E_{\mathrm{ext}} = 1.0$, $A = 1.0$, $f = 1.4$.

The results illustrate that different discharge modes correspond to different energy sequences. The chaotic mode demonstrates a reduced average energy relative to periodic patterns. The relationship between the electric field energy and the magnetic field energy for different external electric fields and sound signals is shown in Fig. 8.

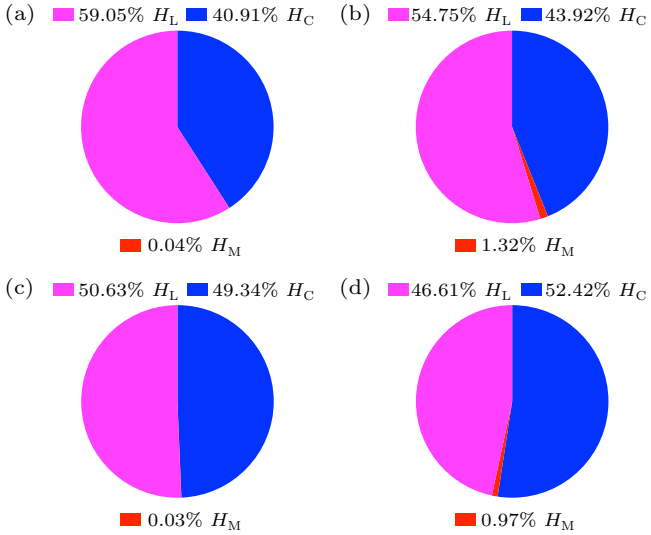


Fig. 8. The energy proportion under different external electric fields and sound signals. (a) $E_{ext} = 0.127$, $A = 0.6$, $f = 1.23$; (b) $E_{ext} = 1.0$, $A = 0.6$, $f = 1.23$; (c) $E_{ext} = 0.127$, $A = 1.0$, $f = 1.4$; (d) $E_{ext} = 1.0$, $A = 1.0$, $f = 1.4$.

From Figs. 7 and 8, these results demonstrate that different firing patterns have different electric–magnetic field energy proportions. The chaotic mode indicates a reduced magnetic field energy proportion relative to periodic patterns. Furthermore, the case of periodic external electric fields is discussed, with E_{ext} considered as $A_1\cos(f_1\tau)$. The external sound signal is $u_{PC} = A\cos(f\tau)$, where $A = 1.0$ and $f = 1.245$. Figure 9 displays a bifurcation diagram of the variable x and LLE under different periodic external electric fields.

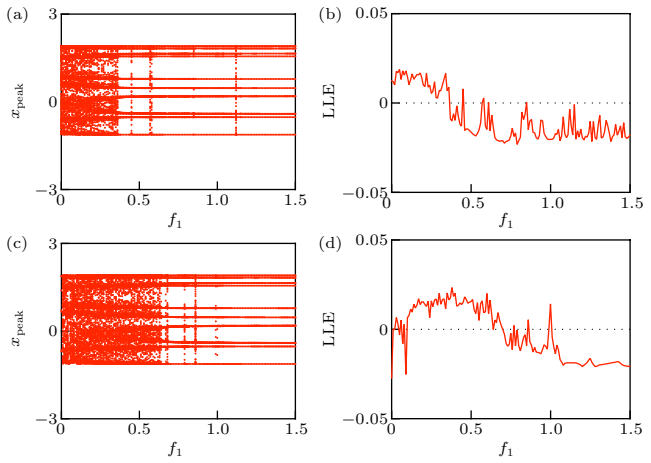


Fig. 9. Bifurcation diagram of the variable x and the LLE for different periodic external electric fields. (a) and (b) $A_1 = 0.5$; (c) and (d) $A_1 = 1.0$.

From Fig. 9, as the frequency of the periodic external electric field increases, the neural network in the chaotic mode evolves into a periodic mode, and the chaotic state is suppressed. As the amplitude of the periodic external electric field increases, the frequency range of the chaotic mode exhibited by the neurons becomes larger than that in the case where the amplitude of the periodic external electric field is smaller. Similarly, Fig. 10 illustrates the distinct firing patterns and corresponding energy evolution under different periodic external electric fields.

The results indicate that different firing patterns correspond to different energy sequences, with the chaotic mode having a smaller average energy and the periodic pattern having a larger average energy. Corresponding to Fig. 10, the energy proportion is displayed in Fig. 11.

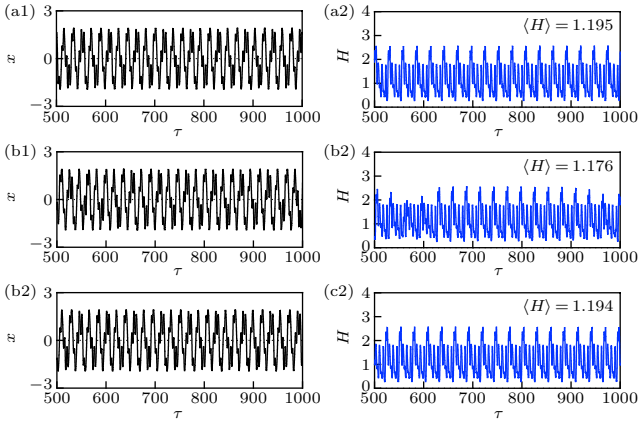


Fig. 10. The membrane potential (x) and the Hamilton energy (H) under different periodic external electric fields. (a1) and (a2) $A_1 = 0.5$, $f_1 = 0.5$; (b1) and (b2) $A_1 = 1.0$, $f_1 = 0.5$; (c1) and (c2) $A_1 = 1.0$, $f_1 = 0.89$.

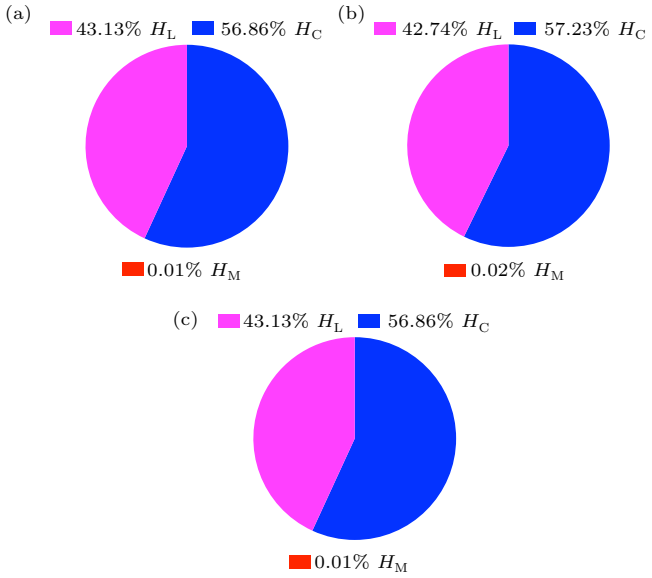


Fig. 11. The energy proportion under different periodic external electric fields. (a) $A_1 = 0.5$, $f_1 = 0.5$; (b) $A_1 = 1.0$, $f_1 = 0.5$; (c) $A_1 = 1.0$, $f_1 = 0.89$.

The results in Fig. 11 show that the periodic pattern has a lower electric field energy proportion and a higher magnetic field energy proportion than that of the chaotic mode. Furthermore, the case of noisy external electric fields is discussed. Parameters and initial values are kept as above, the periodic

external sound signal is $u_{\mathrm{PC}} = \cos(1.245\tau)$, and the sound-sensitive neuron is in a chaotic pattern. To study noise-induced stochastic resonance in neurons driven by periodic sound signals and random electric fields, the signal-to-noise ratio (SNR) and average energy ($\langle H \rangle$) under different Gaussian white noise electric fields are calculated in Fig. 12.

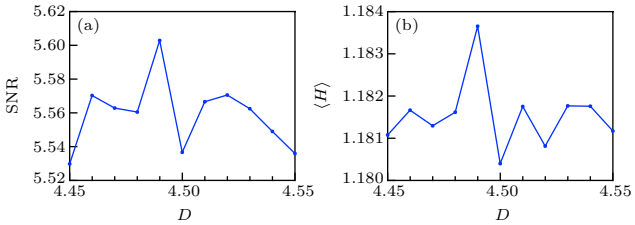


Fig. 12. SNR and $\langle H \rangle$ under different Gaussian white noise electric fields. (a) SNR; (b) $\langle H \rangle$. D represents the Gaussian white noise electric field intensity.

The results illustrate that sound-sensitive neurons with a hybrid memristor ion channel exhibit the phenomenon of stochastic resonance under a Gaussian white noise electric field intensity ($D = 4.49$). The SNR reaches 5.6029, and the average energy reaches 1.1837. Furthermore, to explore the self-regulation characteristics of sound-sensitive neurons with a hybrid memristor–ion channel, the proposed adaptive control mechanism dynamically regulates system energy through real-time monitoring of the electric-to-magnetic field energy ratio ($H_{\mathrm{C}}/H_{\mathrm{L}}$). The method is described as follows:

$$\frac{\mathrm{d}k_{\mathrm{M}}}{\mathrm{d}\tau} = \kappa k_{\mathrm{M}} \theta \left(\varepsilon - \left| \frac{H_{\mathrm{C}}}{H_{\mathrm{L}}} \right| \right),$$
$$\theta(n) = 1, \quad n \geq 0, \quad \theta(n) = 0, \quad n < 0, \tag{13}$$

where k_{M} is a controllable parameter, κ denotes a gain factor, ε is the threshold of the energy ratio, and θ denotes the Heaviside function. Parameters and initial values are kept as above, the periodic external sound signal is $u_{\mathrm{PC}} = \cos(1.23\tau)$, the sound-sensitive neuron is in a chaotic pattern, the initial value of k_{M} is 0.1, and ε is 0.3. The results are shown in Fig. 13.

From Fig. 13, under the adaptive regulation of energy ratios, the parameters can reach a stable value, and the chaotic neurons can self-regulate into a periodic pattern. Furthermore, as the gain coefficient increases, the parameters can reach the stable value more rapidly, and the chaotic mode can quickly adjust to the periodic state.

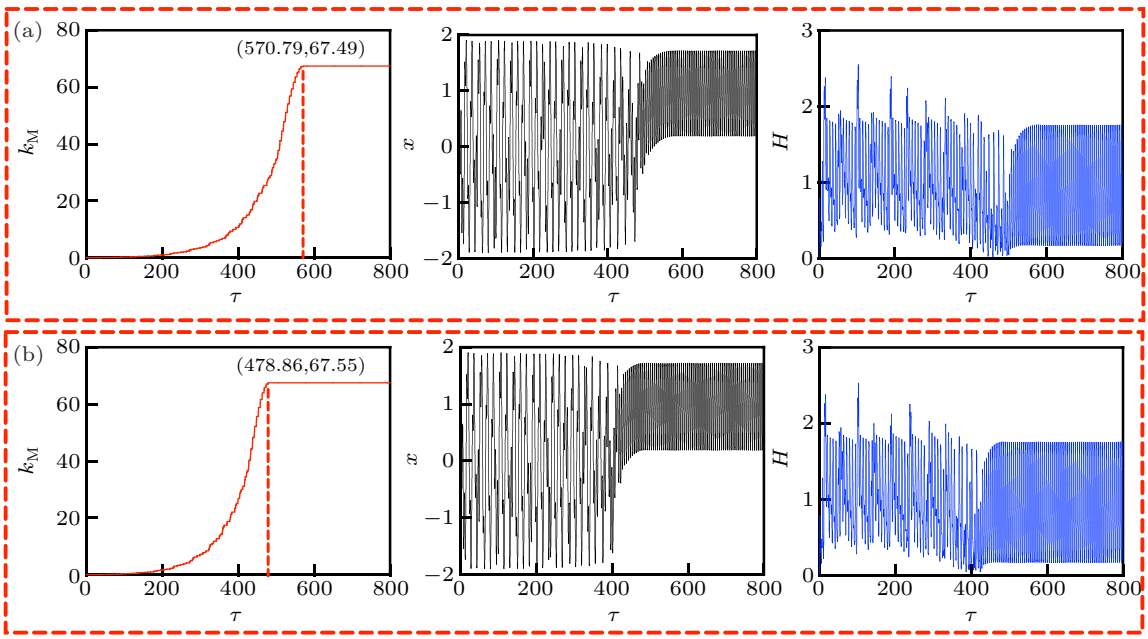


Fig. 13. The self-regulation parameter (k_{M}), membrane potential (x), and Hamilton energy (H) under different gain values κ. (a) $\kappa = 0.05$; (b) $\kappa = 0.06$.

4. Conclusion and perspectives

This study develops a sound-sensitive neural circuit featuring a hybrid ion channel that combines the nonlinear memory properties of memristors with the dynamic characteristics of biological ion channels, followed by a systematic analysis of its dynamical behaviors. The results illustrate that the proposed hybrid memristor–ion channel circuit successfully simulates the frequency-selective response and adaptive emission characteristics of biological neurons to sound signals. Sound-sensitive neurons with a hybrid memristor–ion channel exhibit the phenomenon of stochastic resonance under a Gaussian white noise electric field intensity. In addition, under the adaptive regulation of energy ratios, the parameters can reach a stable value, and the chaotic neurons can self-regulate into a periodic pattern. The hardware circuit implementation of this model is a limitation of this study; however, the model provides new design ideas for neuromorphic engineering, especially in the fields of bionic auditory sensors and edge com-

puting. In the future, the individual neural circuit will be expanded into a network, and its ability to synchronize and separate patterns in complex sound fields (such as noisy environments) will be studied.

Acknowledgment

Project supported by the Youth Innovation Team of Shaanxi Universities.

References

[1] Liu Y, Xu W, Ma J, Alzahrani F and Hobiny A 2020 *Front. Inf. Technol. Electron. Eng.* **21** 1387
[2] Xu Y, Guo Y, Ren G and Ma J 2020 *Appl. Math. Comput.* **385** 125427
[3] Guo Y, Zhou P, Yao Z and Ma J 2021 *Nonlinear Dyn.* **105** 3603
[4] Song X and Yang F 2024 *Phys. Scr.* **99** 125247
[5] Yang F, Guo Q, Ren G and Ma J 2024 *J. Biol. Phys.* **50** 271
[6] Chua L 1971 *IEEE Trans. Circuit Theory* **18** 507
[7] Khalid M 2019 *Trans. Electr. Electron. Mater.* **20** 289
[8] Li Y, Wang Z, Midya R, Xia Q and Yang J J 2018 *J. Phys. D: Appl. Phys.* **51** 503002
[9] Zhang L, Li Z and Peng Y 2024 *Chaos, Solitons Fractals* **185** 115109
[10] Zhang J and Li Z 2024 *Nonlinear Dyn.* **112** 6647
[11] Guo H, Liang Y, Wang G, Li Y, Wang L and Zhao Y 2025 *Int. J. Bifurc. Chaos* **35** 2550075
[12] Shi S, Liang Y, Li Y, Lu Z and Dong Y 2024 *Chaos, Solitons Fractals* **180** 114534
[13] Ma J 2025 *Nonlinear Dyn.* **113** 25365
[14] Yang F, Han Z, Ren G, Guo Q and Ma J 2024 *Eur. Phys. J. Plus* **139** 534
[15] Xie Y, Ye Z, Li X, Wang X and Jia Y 2024 *Cogn. Neurodynamics* **18** 1989
[16] Njitacke Z T, Ramadoss J, Takembo C N, Rajagopal K and Awrejcewicz J 2023 *Chaos, Solitons Fractals* **167** 113014
[17] Yang F, Xu Y and Ma J 2023 *Chaos* **33** 023110
[18] Yang F, Ren G and Tang J 2023 *Nonlinear Dyn.* **111** 21917
[19] Song X and Yang F 2025 *J. Theor. Biol.* **599** 112034
[20] Guo Y, Wu F, Yang F and Ma J 2023 *Chaos* **33** 113106
[21] Wan J, Wu F, Ma J and Wang W 2024 *Chin. Phys. B* **33** 050504
[22] Yang F, Song X and Yu Z 2024 *Chaos, Solitons Fractals* **188** 115496
[23] Yu Z, Zhu K, Wang Y and Yang F 2025 *Chaos, Solitons Fractals* **194** 116233
[24] Yang F, Song X and Yu Z 2025 *Nonlinear Dyn.* **113** 7213
[25] Yang F, Song X and Xu Y 2025 *Chaos, Solitons Fractals* **199** 116740
[26] Jia J, Wang C, Zhang X and Zhu Z 2024 *Chaos, Solitons Fractals* **182** 114738
[27] Yang F, Song X and Ma J 2024 *Chin. J. Phys.* **91** 287
[28] Li Y, Lv M, Ma J and Hu X 2024 *Nonlinear Dyn.* **112** 7541
[29] Fang X, Duan S and Wang L 2023 *Neurocomputing* **517** 93
[30] Huang L, Huang Q, Zang H, Lei T, Fu H and Gao F 2025 *Phys. Scr.* **100** 065232
[31] Chen X, Wang N, Wang Y, Wu H and Xu Q 2023 *Chaos, Solitons Fractals* **174** 113836
[32] Bao B, Hu J, Cai J, Zhang X and Bao H 2023 *Nonlinear Dyn.* **111** 3765
[33] Liu B, Peng X and Li C 2024 *AEU - Int. J. Electron. Commun.* **178** 155283
[34] Bao B, Hu J, Bao H, Xu Q and Chen M 2024 *Cogn. Neurodynamics* **18** 539
[35] Yang F, Ma J and Wu F 2024 *Chaos, Solitons Fractals* **187** 115361
[36] Ren G, Xu Y and Wang C 2017 *Nonlinear Dyn.* **88** 893
[37] Guo Y, Zhu Z, Wang C and Ren G 2020 *Optik* **218** 164993
[38] Xie Y, Wang X, Li X, Ye Z, Wu Y, Yu D and Jia Y 2024 *Chin. J. Phys.* **90** 64
[39] Yang F and Ma J 2023 *Pramana* **97** 55
[40] Xie Y, Yao Z and Ma J 2022 *Front. Inf. Technol. Electron. Eng.* **23** 1407
[41] Xie Y, Yao Z and Ma J 2023 *Sci. China Technol. Sci.* **66** 439
[42] Yang F, Wang Y and Ma J 2023 *Commun. Nonlinear Sci. Numer. Simul.* **119** 107127
[43] Yang F, Hu X, Ren G and Ma J 2023 *Eur. Phys. J. B* **96** 80
[44] Njitacke Z T, Takembo C N, Awrejcewicz J, Fouda H P E and Kengne J 2022 *Chaos, Solitons Fractals* **160** 112211
[45] Wang C, Lv M, Alsaedi A and Ma J 2017 *Chaos* **27** 113108